Biopolymer nanocomposites based on poly(hydroxybutyrate-co-hydroxyvalerate) reinforced by a nonionic organoclay

Larissa N. Carli, Tales S. Daitx, Régis Guégan, Marcelo Giovanela, Janaina S. Crespo, Raquel S. Mauler

Biopolymer nanocomposites based on poly(hydroxybutyrate-co-hydroxyvalerate) reinforced by a nonionic organoclay

Larissa N. Carli[a,*,#], Tales S. Daitx[b], Régis Guégan[c,d,*], Marcelo Giovanela[a], Janaina S. Crespo[a], Raquel S. Mauler[b,*]

[a] Centro de Ciências Exatas e Tecnologia, Universidade de Caxias do Sul, Rua Francisco Getúlio Vargas, 1130, Caxias do Sul, 95070-560, RS, Brazil – larissa.carli@gmail.com; mgiovan1@ucs.br; jscrespo@ucs.br

[b] Instituto de Química, Universidade Federal do Rio Grande do Sul, Av. Bento Gonçalves, 9500, Porto Alegre, 91501-970, RS, Brazil – tales.daitx@ufrgs.br; raquel.mauler@ufrgs.br

[c] Institut des Sciences de la Terre d'Orléans, UMR 7327 CNRS-Université d'Orléans, 1A Rue de la Ferollerie, 45071 Orléans Cedex 2, France – regis.guegan@univ-orleans.fr

[d] Graduate School of Creative Science and Engineering, Waseda University, Nishiwaseda 1-6-1, Shinjuku, Tokyo, 169-8050, Japan

This article has been accepted for publication and undergone full peer review but has not been through the copyediting, typesetting, pagination and proofreading process, which may lead to differences between this version and the Version of Record. Please cite this article as doi: 10.1002/pi.4781

* Author to whom correspondence should be addressed: Phone/Fax: +55 51 3308 6296
E-mail:larissa.carli@gmail.com, raquel.mauler@ufrgs.br, regis.guegan@univ-orleans.fr

Present address: Campus Blumenau, Universidade Federal de Santa Catarina, Rua Pomerode, 710, Blumenau, 89065-300, SC, Brazil (L. N. Carli)

Abstract. In this study, a nanocomposite based on a biodegradable polymer poly(hydroxybutyrate-co-hydroxyvalerate) (PHBV) reinforced by triethylene glycol mono-n-decyl ether ($C_{10}E_3$) nonionic organoclay ($C_{10}E_3$-Mt) was prepared. The morphology and the thermal and mechanical properties of PHBV/$C_{10}E_3$-Mt were compared with those of PHBV nanocomposites prepared using commercial organically modified montmorillonite Cloisite® 30B (OMt) and raw montmorillonite (Mt). Nanocomposites with 3 wt % nanoparticles were obtained by melt processing. The high level of dispersion with improved interfacial interactions between OMt and polymer led to an increase in the thermal stability and modulus of PHBV. However, this nanocomposite presented a lower strain before fracture, typical of brittle behavior. The transmission electron microscopy (TEM) and wide angle X-ray diffraction (WAXD) results revealed a significant increase in the interlayer spacing of clay for the PHBV/$C_{10}E_3$-Mt nanocomposite, which was favored by the wide expansion of the platelets of the starting nonionic organoclay. This characteristic of $C_{10}E_3$-Mt, together with its hydrophobic behavior, allowed its easy incorporation in the PHBV matrix, thus improving the processing and maintaining a high modulus with increased material toughness.

Keywords: Biodegradable polymer, Nanocomposites, Nonionic organoclay, Thermomechanical properties, Impact strength

Introduction

Polymer-based nanocomposites are recognized as promising materials due to the possible and versatile modifications of the performance of the materials by the incorporation of small amounts of nanosized inorganic particles. In this way, for well-dispersed clay mineral layers, even with low contents in the polymer matrix, polymer-clay nanocomposites exhibit useful properties, such as mechanical strength, thermal stability, gas barrier, flame retardancy and biodegradability [1].

Poly(hydroxybutyrate-co-hydroxyvalerate) (PHBV), a member of polyhydroxyalkanoates (PHA) polyester class, has been shown to be a potential environmentally friendly substitute for traditional plastics [2, 3]. The incorporation of several reinforcing nanoparticles into PHBV, using a solution intercalation method [4-6] and, more recently, by melt mixing [7-9], which enhances its mechanical and thermal properties, has been extensively studied in past years. The reference fillers for the polymer matrix are organoclays prepared using conventional cationic surfactants, such as alkylammonium ions. Depending on the surfactant concentration in regards to the cation exchange capacity of swelling clay minerals, such as montmorillonite (Mt), several packing arrangements (monolayer, bilayer and even trilayers) could be observed. These different packing arrangements lead to an expansion of the interlayer galleries and drive the surface to have an organophilic nature which are key parameters for a good dispersion or exfoliation of Mt layers in the polymer matrix [1].

Although the final properties of PHBV nanocomposites were enhanced, several studies showed less interest in using conventional organoclays for several reasons: (i)

organic ammonium cations undergo thermal degradation at temperatures greater than 170-180 °C, which consequently restrains their potential engineering applications [10]; (ii) the incorporation of such cationic surfactants favors the degradation of PHBV, leading to a lack of performance of the nanocomposites [11, 12]; and (iii) the cationic surfactant is highly toxic, which prevents the safe biodegradation of PHBV nanocomposites [13].

Research interest has recently shifted towards the use of different clay mineral-like halloysites as fillers [14, 15], and even as other organo-modifiers, including nonionic surfactants [16]. Indeed, nonionic surfactants containing n-C_nH_{2n+1}-$(OCH_2CH_2)_m$OH surfactants were demonstrated to be chemically and thermally stable, biodegradable, non-toxic, and non-corrosive [17, 18]. In contrast to ammonium salts, for which the intercalation invokes electrostatic interactions, the adsorption of nonionic surfactants onto Mt involves several interaction mechanisms, such as H-bonds, ion-dipole interactions and Van der Waals interactions that stabilize the resulting organoclay [19-22]. Although the main driving force leading to adsorption has not yet been clearly established and is still under controversy, nonionic surfactants and other associated relative poly(oxyethylene)s could be successfully intercalated in Mt, expanding the interlayer space to a distance of 1.4 and 1.8 nm, corresponding to lateral monolayer and bilayer packing, respectively [19-23]. Recently, the use of the triethylene glycol mono-n-decyl ether ($C_{10}E_3$) as organo-modifiers has attracted attention. Indeed, the adsorption of this nonionic surfactant onto Mt above the critical micelle concentration, in which the $C_{10}E_3$ self-assembles into a lamellar phase, leads to the intercalation of a normal bilayer (d_{001} spacing of ≈ 36.4 Å) arrangement, resulting in a condensation of the bulk lamellar phase [24, 25]. This nonionic organoclay exhibits a wide expansion of its interlayer space

while simultaneously having a hydrophobic surface, which makes its dispersion or exfoliation easier compared to previous, similar system fillers in the polymer matrix.

Thus, this work aims to develop novel PHBV nanocomposites reinforced with a nonionic organoclay and to evaluate and compare their mechanical and thermal properties to a PHBV nanocomposite in which organically modified Mt Cloisite® 30B (OMt) and raw Mt particles were used as the filler. This paper provides interesting information on the properties of polymer nanocomposites with nonionic organoclays used as fillers.

Experimental

Materials

PHBV, with a viscosimetric molecular weight of 340000 g mol^{-1} and a valerate content of 2 % (estimated using ^{1}H NMR solution ($CDCl_3$) spectroscopy), was supplied by Ningbo Tianan Biologic Material Co., Ltd. (ENMAT Y 1000). The commercial clay mineral was a purified montmorillonite (Mt) provided by Kunipia Kunimine Industries. The triethylene glycol mono-*n*-decyl ether ($C_{10}E_3$) nonionic surfactant was purchased from Nikko Chemicals Inc. and was used without further purification. The cationic organoclay, which was used as a reference material, was an organo-modified montmorillonite Cloisite® 30B (OMt) containing a methyl *bis*-2-hydroxyethyl ammonium quaternary salt. This organoclay had a cation exchange capacity (CEC) of 90 meq/100 g and was supplied by Southern Clay Products.

Preparation of nonionic organoclay

An aqueous solution of $C_{10}E_3$ was prepared at room temperature at a starting concentration of 10^{-2} mol L^{-1}, at which $C_{10}E_3$ self-assembles into a lamellar phase. 50 mL of a Mt suspension solution (concentration 60 g L^{-1}) was then dispersed into 50 mL of the surfactant solution, and the suspension was stirred overnight at 250 rpm. In this way, $C_{10}E_3$ was intercalated in a bilayer arrangement, expanding the interlayer space of Mt, as previously observed [24, 25]. The nonionic organoclay ($C_{10}E_3$-Mt) was then separated by centrifugation and dried at 70 °C for 48 h before being crushed using an agate mortar.

Melt processing

All materials used in this study were dried under vacuum at 80 °C for 6 h before use. The content of nanoparticles used was 3 wt%, based on the results of our previous work [14]. The PHBV nanocomposites were obtained using a Haake Rheomix 600p internal mixer operating at 100 rpm and 170 °C for 7 min, with a torque precision of ± 0.5 N m.

The mechanical energy (E_m) (kJ kg^{-1}) was calculated from the torque *vs*. time curves using Equation 1:

$$E_m = \left(\frac{N}{M}\right) \cdot S \qquad (1)$$

where N is the rotation speed (rad s^{-1}), M is the sample mass (kg) introduced in the mixing chamber and S is the area defined by the torque *vs*. time curve (N m s).

The nanocomposites were injection molded in a Haake MiniJet II mini injection molding machine. The temperature of the cylinder was maintained at 190 °C, and the mold was maintained at 80 °C. For reference, neat PHBV and PHBV nanocomposites with unmodified Mt were also processed and analyzed under the same conditions.

Nanocomposites characterization

The morphology of the nanocomposites was examined by transmission electron microscopy (TEM) using a JEOL JEM-1200 Ex II microscope operating at an accelerating voltage of 80 kV. Ultra-thin specimens (70 nm) were cut from the middle section of molded samples in a direction perpendicular to the flow of the melt during the injection process. The cut was performed under cryogenic conditions using a RMC PowerTome XL ultramicrotome with a RMC CRX cryosectioning attachment and operating a diamond knife at -80 °C; the films were retrieved on 300 mesh Cu grids.

Wide angle X-ray diffraction (WAXD) measurements were performed using a Siemens D-500 diffractometer operating in reflection mode geometry with incident Cu K_α radiation (λ = 1.5405 Å). The d_{001} basal spacing of the injection-molded samples was measured at room temperature in step-scanning mode from 2θ = 1° to 45° with a step size of 0.05° min^{-1}.

The crystallization characteristics were determined by differential scanning calorimetry (DSC) using a TA Instruments DSC Q-20. The samples were analyzed from 30 °C to 200 °C at a heating and cooling rate of 10 °C min^{-1} under nitrogen flow. The measurements were performed during the first cooling scan and during the second heating scan. The degree of crystallinity (X_c) of the PHBV matrix and nanocomposites was determined as follows:

$$X_c = \frac{\Delta H_m}{f_p \cdot \Delta H_m^o} \times 100 \qquad (2)$$

where ΔH_m (J g^{-1}) is the melting enthalpy of the polymer matrix, f_p is the polymer weight fraction (PHBV) in the sample and ΔH_m^o is the melting enthalpy of pure

crystalline PHBV (ΔH_m^o = 146 J g^{-1}) [26]. The DSC instrument was calibrated with indium before use.

The thermal stability of the nanocomposites was evaluated by thermogravimetric analyses (TGA). TGA was conducted using a TA Instrument QA-50. The samples were heated from 25 °C to 700 °C at a heating rate of 20 °C min^{-1} under nitrogen flow.

The mechanical properties were evaluated through dynamic mechanical analyses (DMA) and impact strength measurements. DMA analyses were performed in single cantilever mode in a TA model QA 800 Instrument. The injection-molded samples were heated from -30 °C to 120 °C at 3 °C min^{-1}. The experiment was conducted within the linear viscoelastic region using a small amplitude (0.1%) and the frequency was set at 1 Hz for all samples. The instrumented notched Izod impact tests were performed according to ASTM D 256-06a on a pendulum-type Ceast 6545 at 23 °C with a data acquisition unit and a maximum work capacity of 2.75 J. Five specimens were analyzed, and the average and standard deviation were calculated.

Results and discussion

Melt processing

Figure 1 shows the torque *vs*. time curves obtained from the melt processing in the internal mixer. The calculated values of the stabilized torque and total mechanical energy of the PHBV and PHBV nanocomposites are presented in Table 1.

It is possible to observe that the neat PHBV and PHBV/$C_{10}E_3$-Mt show similar behavior, with torque decreasing with time and reaching a plateau regime of approximately 2.0 N m at the end of the melt processing. The mechanical energy, calculated from the torque vs. time curves, is slightly higher for PHBV/$C_{10}E_3$-Mt

nanocomposite compared to neat PHBV, PHBV/Mt and PHBV/OMt. Since the mechanical energy is connected to the viscosity [11], the slightly high viscosity of the PHBV/$C_{10}E_3$-Mt system is an indicative that the presence of $C_{10}E_3$-Mt inhibits the thermal degradation of this sample during processing.

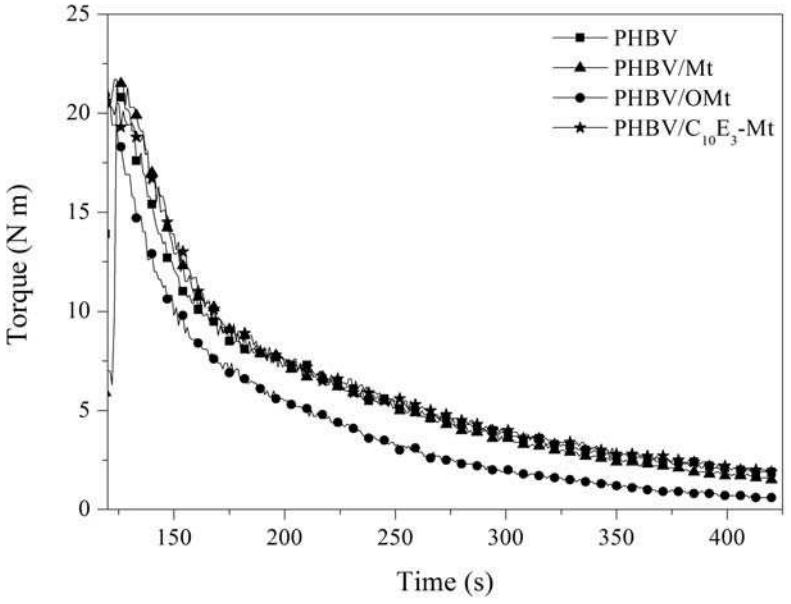

Figure 1. Torque *vs*. time curves for PHBV and PHBV nanocomposites.

However, it is possible to observe that the torque decreases more rapidly in the PHBV/OMt nanocomposite, with torque values close to zero at the end of the melt processing. The low viscosity of this nanocomposite is most likely a direct consequence of the degradation of PHBV in the presence of quaternary ammonium salts, as previously demonstrated by Hablot et al [11] and Bordes et al [12]. At the processing temperature, the ammonium surfactants can decompose through Hofmann elimination or through nucleophilic attack of the counter-ion on the quaternary ammonium. The decomposition products can enhance the degradation reaction of PHB or PHBV [27].

These results confirm the best thermal stability of neat PHBV and PHBV/$C_{10}E_3$-Mt nanocomposites during melt processing.

Morphology

Figure 2 shows the TEM images of the PHBV nanocomposites. The TEM image of the PHBV/OMt nanocomposites indicates the disruption of the clay aggregates, with the presence of elongated structures with greater separation between platelets, which are homogeneously dispersed in the PHBV matrix. The nanocomposites with Mt and $C_{10}E_3$-Mt also show a good dispersion of the clay platelets in the PHBV matrix. However, it is also possible to observe the occurrence of some aggregates of silicate layers. The WAXD analysis was performed to evaluate these findings, as shown in Figure 3.

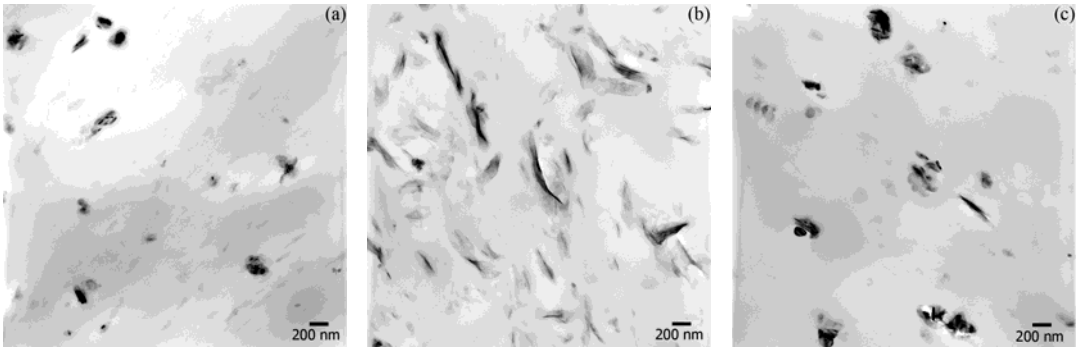

Figure 2. TEM micrographs of (a) PHBV/Mt, (b) PHBV/OMt, and (c) PHBV/$C_{10}E_3$-Mt nanocomposites.

Figure 3 shows the diffraction patterns of the unmodified Mt, organoclays and their related polymer nanocomposites. The diffraction patterns of the organoclays present the 001 reflection at lower diffraction angles, suggesting successful intercalation within the interlayer space of quaternary ammonium and $C_{10}E_3$ compounds. The d_{001} basal spacing of the starting reinforcement materials are 1.0, 1.8 and 3.6 nm for

dehydrated Mt, OMt and $C_{10}E_3$-Mt, respectively. Computer simulation and previous X-ray diffraction experiments showed that the swelling of Mt corresponds to four stable states at basal spacing of 0.97, 1.2, 1.55, and 1.82 nm due to the hydration of one, two, and three water molecules around the exchangeable inorganic cations, respectively [28, 29]. The value of 1.0 nm demonstrates that the Mt is in a dehydrated state. The commercial organoclay used in this study was prepared at a CEC concentration for which all counter ions were substituted by organic cations, leading to a lateral bilayer arrangement, as previously reported in many studies. In contrast to the commercial organoclay, the nonionic organoclay exhibited a wide expansion of the interlayer space due to a condensation of the lamellar phase during the preparation of the organoclay.

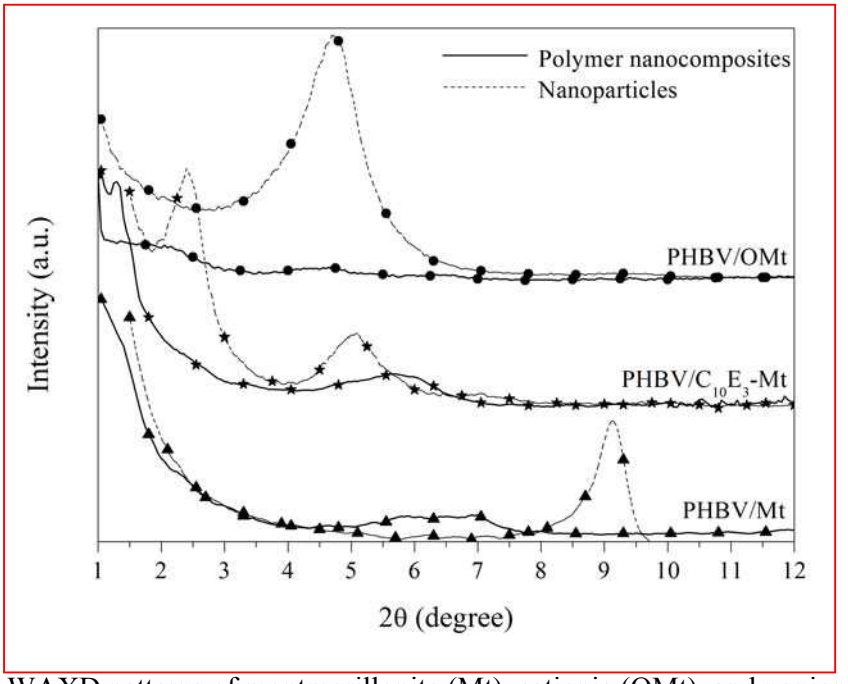

Figure 3. WAXD patterns of montmorillonite (Mt), cationic (OMt), and nonionic ($C_{10}E_3$-Mt) organoclays as reinforcement materials in polymer and the associated PHBV nanocomposites.

The PHBV/Mt nanocomposite exhibits a shift of the 001 diffraction peak of Mt to lower angles, indicating an increase of the interlayer distance to 1.38 nm. This displacement suggests that the Mt layers were intercalated by the polymer chains. The PHBV/OMt nanocomposites show a broadening of the first reflection, which can be attributed to a reduction in the coherent layer stacking length [30]. This reduction may account for the formation of a more disordered structure, most likely with exfoliated clay domains. Similarly, PHBV/$C_{10}E_3$-Mt shows an increase of the d_{001} spacing to a value of 6.84 nm (reflection at 1.5°) compared to the 001 reflection at 2.5° and its second order at 5° of the $C_{10}E_3$-Mt organoclay, where the d_{001} spacing matches the thickness of a $C_{10}E_3$ bilayer as it was previously reported [24]. Such increase of the d_{001} spacing suggests that the polymer was intercalated within the interlayer space. The wide expansion of the platelets of the starting nonionic organoclay favors the intercalation of the polymer chains into the intergallery, maintaining an ordered structure. Nevertheless, another broad reflection with a maximum at approximately 6° (2θ) can be distinguished, which does not match any other orders of the first reflection at low angle values. The presence of such a diffraction peak corresponding to an interlayer spacing of 1.35 nm suggests a collapse of the clay layers with a reorganization of $C_{10}E_3$ in lateral monolayer due to a possible removing of the surfactant in some intergalleries once the nonionic organoclay is added in PHBV matrix. Moreover, it is probable that the particular affinity between the PHBV polymer and the surfactant involving Van der Waals interaction and H-bonds, as well as the envelopment of the organoclay layers by the polymer chains, contributes to the escape of surfactant molecules and its diffusion within the polymer chains. This fact corroborates the plasticizing effect with the addition of $C_{10}E_3$-Mt on the PHBV, as discussed later.

Crystallization characteristics

DSC analyses were conducted to study the influence of Mt on the non-isothermal crystallization behavior of the PHBV nanocomposites. Figure 4 shows the results of the DSC analyses of the PHBV and PHBV nanocomposites. The surface of raw Mt does not induce any nucleation effect for the crystallization of PHBV, even without any organic modification, because an increase was not observed in the crystallization temperature (T_c) of the nanocomposites (Table 2).

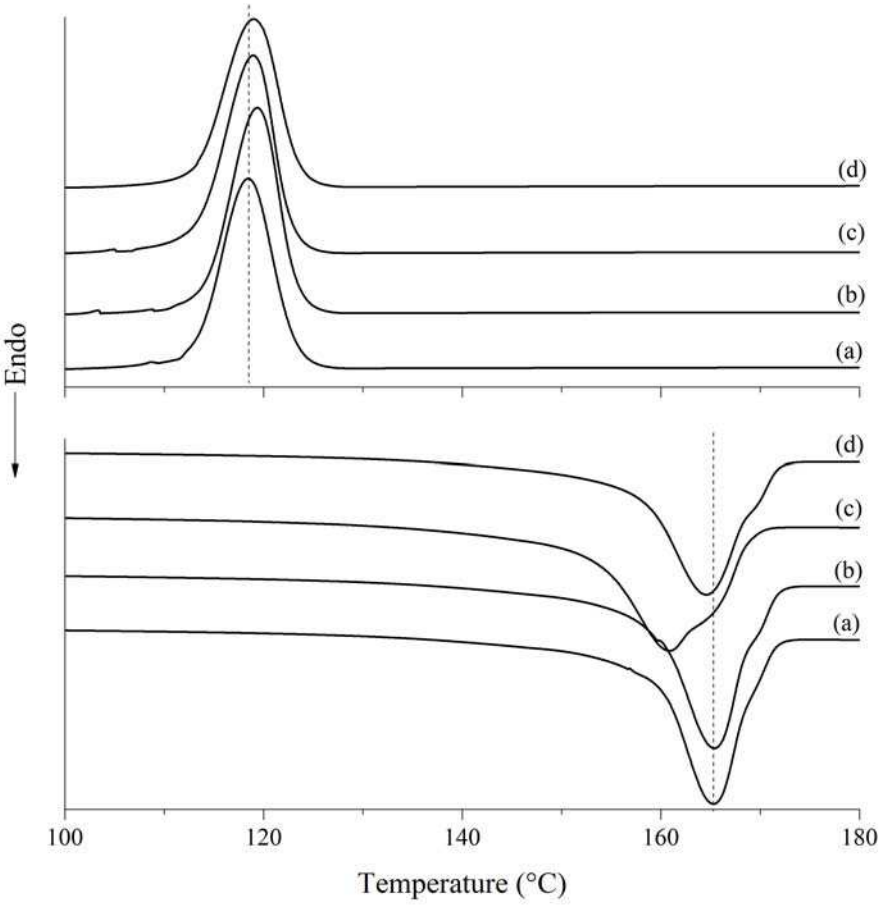

Figure 4. DSC curves of (a) PHBV and (b) PHBV/Mt, (c) PHBV/OMt, and (d) PHBV/$C_{10}E_3$-Mt nanocomposites (temperature error: ± 1.0 °C).

In contrast, the melting of the nanocomposites prepared by both organoclays behaves differently following the nature of surfactants used (Figure 4). For PHBV/OMt, a shift to low temperature for T_m and a broadening of the melting enthalpy peak could be observed. This effect has previously been discussed [14, 31] and was attributed to the formation of smaller and/or less perfect crystals as a consequence of the polymer degradation during processing in the presence of quaternary ammonium salts as an organo-modifier of the clay mineral. The nanocomposites with raw Mt and $C_{10}E_3$-Mt show similar behavior to the unreinforced polymer, indicating that the surfaces of the introduced species do not affect the crystallization process of the polymer matrix.

Thermal stability

The thermal stability of the nanocomposites was evaluated using TGA. Figure 5 presents the TGA and DTG curves of the neat PHBV and PHBV nanocomposites.

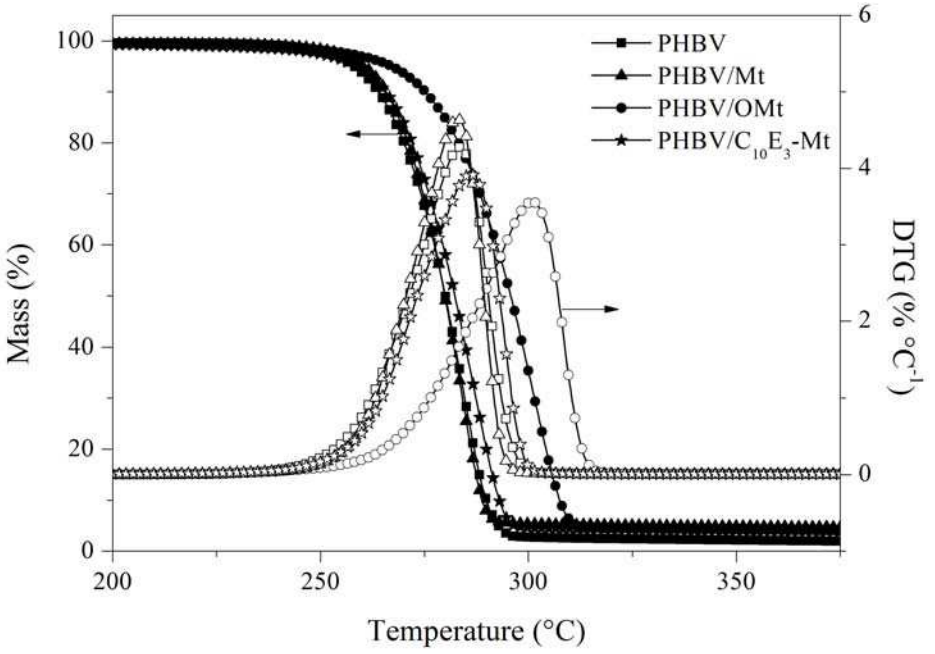

Figure 5. TGA and DTG curves of PHBV and PHBV nanocomposites (temperature error: ± 0.5 °C; mass error: 0.6%).

All the nanocomposites behave similarly to the neat polymer, i.e., the thermal degradation consisted of only one weight loss step between 250 °C and 320 °C in accordance with the non-radical, random chain scission reaction [32]. This indicates no change in the degradation mechanism of the PHBV with the incorporation of nanoparticles. The characteristic temperatures $T_{5\%}$ and T_p, which correspond to the initial decomposition temperature (5% of degradation) and to the maximum degradation rate, respectively, and the inorganic content are shown in Table 2.

The best dispersion and the strong interaction of OMt in the PHBV matrix has most likely created a barrier effect towards polymer degradation products, which lead to an increase of 18 °C in the thermal stability of the PHBV/OMt nanocomposites. This barrier effect clearly counterbalanced the degradation effects of the quaternary ammonium salts. The presence of some agglomerated structures for PHBV/Mt and PHBV/$C_{10}E_3$-Mt, as observed in the TEM images, did not promote this effect, which was reflected by values similar to those of the neat polymer. The residue remaining at 600 °C was consistent with the theoretical clay content.

Mechanical properties

Figure 6 shows the storage modulus (E'), loss modulus (E") and tan δ curves from the DMA analysis for the PHBV and PHBV nanocomposites. The storage modulus reflects the capability of a material to store mechanical energy and resist deformation, while the loss modulus reflects the ability to dissipate energy [33]. The addition of

nanoparticles to PHBV increased the E' and E" of the system over the entire temperature range and was independent of the modification of the clay mineral. The increase in E' was more pronounced at temperatures above the glass transition temperature (T_g) determined from the tan δ peak. Above the T_g, the nanoparticles, through their interaction with the polymer chains, restrained the motion of the polymer, leading to an increase of E'. Below the T_g, the PHBV/Mt nanocomposite presented a more pronounced increase in the storage modulus. However, the PHBV/OMt nanocomposite presented a high stiffness at high temperatures. The highest increase of E' due to the addition of OMt can be attributed to high levels of dispersion with improved interfacial interactions between the surface of the clay mineral and the polymer matrix, which are related to the strong interaction between OMt and PHBV, as previously observed by Fukushima et al [34] for PLA and PCL nanocomposites.

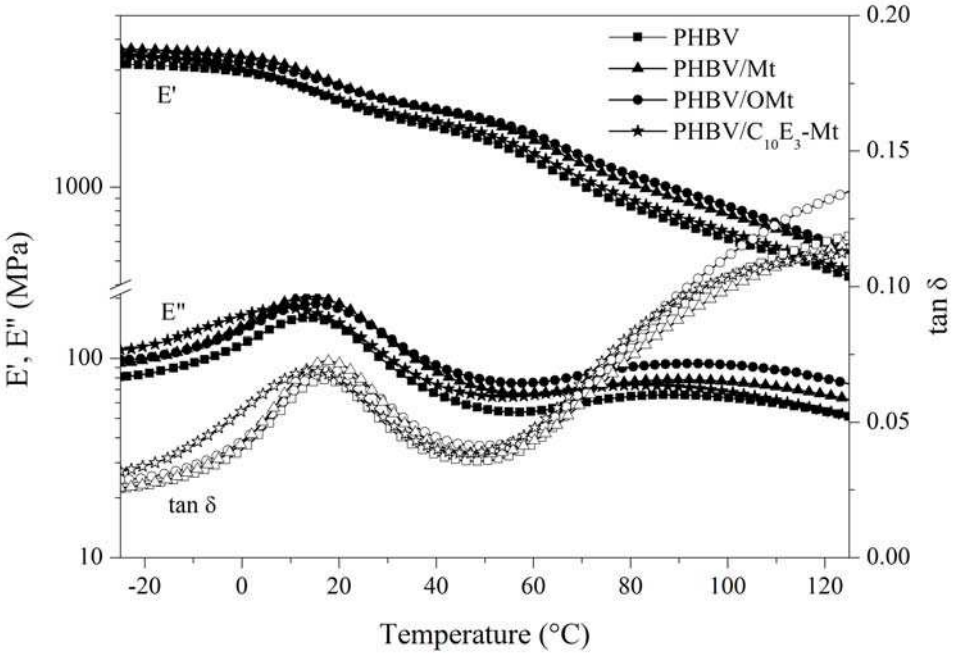

Figure 6. DMA curves of PHBV and PHBV nanocomposites (temperature error: ± 0.5 °C).

The T_g of a polymer depends on the mobility of the chain segment of the macromolecules in the polymer matrix. If the molecular chain is restricted due to the homogeneous dispersion of clay minerals and the interactions between the filler and polymer matrix, motion or relaxation of the chain segment becomes difficult, thus increasing the glass transition temperature [35]. The T_g of neat PHBV and PHBV nanocomposites was similar.

The only exception was the system containing $C_{10}E_3$-Mt, for which the T_g decreased marginally with the formation of the nanocomposite. Such behavior can be attributed to a plasticizing effect of the nonionic surfactant. The fraction of surfactant that left the interlayer space of the clays may be interacting with the polymer chains, thus increasing the molecular interchain spacing of PHBV. Such effect may be inverted for organoclays with low surfactant density and lateral arrangement as OMt showed. In the tan δ curve, the second high temperature wide peak can be associated with the phenomena such as intracrystalline relaxation and sliding of tied chains within crystalline blocks. This behavior can be frequently observed for semicrystalline polymers such as polypropylene and polyethylene [36-38]. This transition helps extend the operating range of a material above the T_g [36].

Figure 7 presents the instrumented impact results, which relates the force and energy absorbed by the PHBV nanocomposites.

The overall fracture process may be divided into both crack initiation and propagation stages [39]. The maximum force is the highest load where crack initiation occurs. Thus, the peak force can also be presumed as a threshold beyond which the material fractures [40]. Relatively low values of the maximum load are observed for the

PHBV/Mt nanocomposite. The maximum load remains similar for all other samples. On the other hand, the PHBV/OMt nanocomposite exhibited a much lower strain before fracture, as indicated by the smaller amount of time to reach fracture. This sample was essentially elastically loaded until failure, as represented by the sudden decrease in load to a near zero value. This is characteristic of brittle fracture, with an approximately linear loading curve that ends in a sharp drop after reaching the maximum load [39, 41].

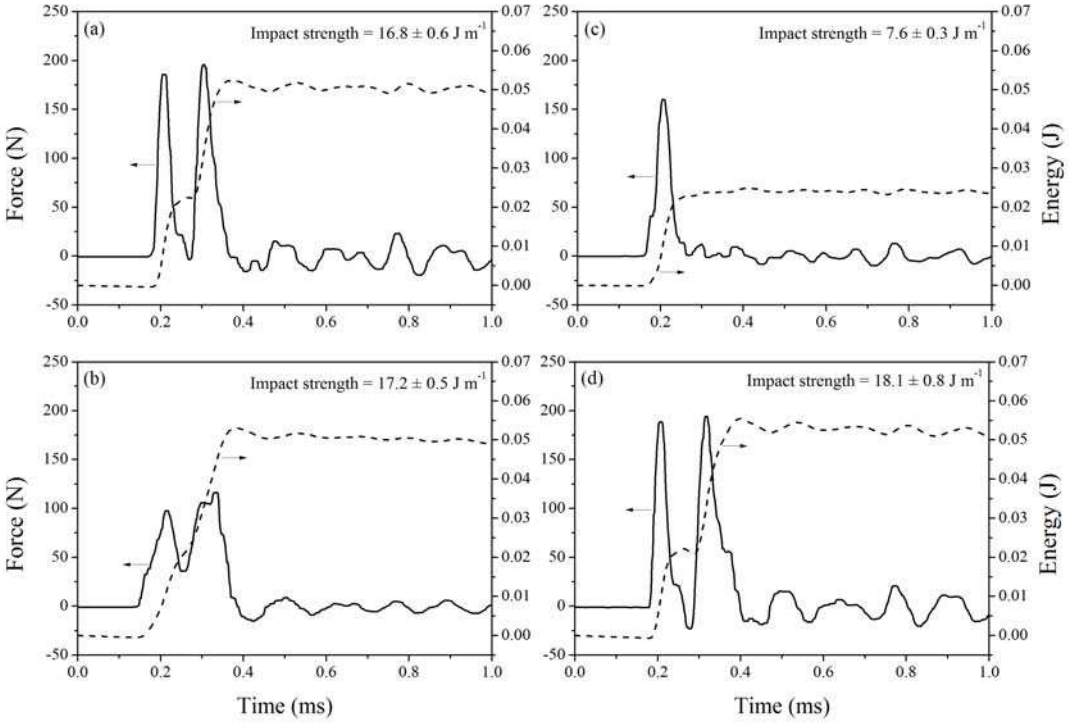

Figure 7. Force and absorbed energy *vs*. time curves of (a) PHBV, (b) PHBV/Mt, (c) PHBV/OMt, and (d) PHBV/$C_{10}E_3$-Mt nanocomposites from the instrumented impact tests.

The conventional total breaking energy is the total fracture energy absorbed during the test and is represented by the area under the force-time curve [40]. This fracture energy is not only dissipated in the crack-initiation stage but is also required for the

crack-propagation stage. It is possible to observe that the neat PHBV, PHBV/Mt and PHBV/$C_{10}E_3$-Mt nanocomposites absorb approximately two times more energy as the PHBV/OMt nanocomposite. This result corroborates the brittle behavior of the latter. The higher energy absorption during the entire fracture process presented by PHBV/$C_{10}E_3$-Mt suggests a higher toughness of the sample.

The impact strength values are also presented in Figure 7. The results confirm that the impact strength values were markedly reduced by the incorporation of OMt. This property loss can be attributed to the degradation of PHBV during processing, as observed in the torque curves. However, the PHBV/$C_{10}E_3$-Mt nanocomposite showed a slight increase in the impact strength, which can be attributed to the plasticizing effect of the surfactant.

Conclusions

In this study, biopolymer degradable nanocomposites based on PHBV and a nonionic organoclay were successfully obtained by melt mixing. The intercalation of the $C_{10}E_3$ nonionic surfactant into Mt provided a high separation of clay platelets and promoted the intercalation of the polymer chains into the interlayer space of Mt. In comparison to OMt, the formation of a well-organized intercalated structure, together with the good interaction between the nonionic surfactant and the polymer chain, was responsible for the improvement in the processing of the polymer and the mechanical properties. Thermo-mechanical analysis indicated a plasticizing effect of $C_{10}E_3$-Mt in the PHBV matrix. This plasticizing effect improved the toughness of the materials without affecting their high modulus value.

The organic modification of nanoparticles using nonionic surfactants provides clay minerals with increased adsorption capacity, control over the interlayer spacing and higher chemical stability compared to commercial cationic organoclays. The results of this study can open new prospects for the preparation of biodegradable polymer nanocomposites.

Acknowledgements

The authors are grateful to Secretaria da Ciência e Tecnologia do Estado do Rio Grande do Sul (SCT), Conselho Nacional de Desenvolvimento Científico e Tecnológico (CNPq), Pronex (FAPERGS/CNPq), and UFRGS (Edital PROPG n° 001/2011) for financial support. Moreover, the co-author Régis Guégan is grateful to the Canon Foundation in Europe for their support in this research allowing him to be hosted at the University of Waseda.

References

[1] Theng BKG. Formation and properties of clay-polymer complexes. 2 ed.Elsevier, Amsterdam, (2013).

[2] Lee SY. *Biotechnol Bioeng* **49:** 1-14 (1996).

[3] Song C, Zhao L, Ono S, Shimasaki C and Inoue M. *Appl Biochem Biotechnol* **94:** 169-178 (2001).

[4] Lai M, Li J, Yang J, Liu J, Tong X and Cheng H. *Polym Int* **53:** 1479-1484 (2004).

[5] Wang S, Song C, Chen G, Guo T, Liu J, Zhang B and Takeuchi S. *Polym Degrad Stab* **87:** 69-76 (2005).

[6] Dagnon KL, Chen HH, Innocentini-Mei L and D'Souza NA. *Polym Int* **58:** 133-141 (2009).

[7] Botana A, Mollo M, Eisenberg P and Sanchez RMT. *Appl Clay Sci* **47:** 263-270 (2010).

[8] Bordes P, Pollet E, Bourbigot S and Avérous L. *Macromol Chem Phys* **209:** 1473-1484 (2008).

[9] Choi WM, Kim TW, Park OO, Chang YK and Lee JW. *J Appl Polym Sci* **90:** 525-529 (2003).

[10] Beall GW and Goss M. *Appl Clay Sci* **27:** 179-186 (2004).

[11] Hablot E, Bordes P, Pollet E and Avérous L. *Polym Degrad Stab* **93:** 413-421 (2008).

[12] Bordes P, Hablot E, Pollet E and Avérous L. *Polym Degrad Stab* **94:** 789-796 (2009).

[13] Shen Y-H. *Chemosphere* **44:** 989-995 (2001).

[14] Carli LN, Crespo JS and Mauler RS. *Compos Part A* **42:** 1601-1608 (2011).

[15] Carli LN, Daitx TS, Soares GV, Crespo JS and Mauler RS. *Appl Clay Sci* **87:** 311-319 (2014).

[16] Sarier N and Onder E. *Thermochim Acta* **510:** 113-121 (2010).

[17] Mathur S and Moudgil BM. *J Colloid Interface Sci* **196:** 92-98 (1997).

[18] Burchill S, Hall PL, Harrison R, Hayes MHB, Langford JI, Livingston WR, Smedley RJ, Ross DK and Tuck JJ. *Clay Miner* **18:** 373-397 (1983).

[19] Su C-C and Shen Y-H. *Colloids Surf, A* **312:** 1-6 (2008).

[20] Su C-C and Shen Y-H. *J Colloid Interface Sci* **332:** 11-15 (2009).

[21] Guégan R, Gautier M, Beny J-M and Muller F. *Clays Clay Miner* **57:** 502-509 (2009).

[22] Deng Y, Dixon JB and White GN. *Colloid Polym Sci* **284:** 347-356 (2006).

[23] Deng Y, Dixon JB and White GN. *Clays Clay Miner* **51:** 150-161 (2003).

[24] Guégan R. *Langmuir* **26:** 19175-19180 (2010).

[25] Guégan R. *Soft Matter* **9:** 10913-10920 (2013).

[26] Gogolewski S, Jovanovic M, Perren SM, Dillon JG and Hughes MK. *Polym Degrad Stab* **40:** 313-322 (1993).

[27] Xie W, Gao Z, Pan W-P, Hunter D, Singh A and Vaia R. *Chem Mater* **13:** 2979-2990 (2001).

[28] Karaborni S, Smit B, Heidug W, Urai J and van Oort E. *Science* **271:** 1102-1104 (1996).

[29] Ferrage E, Lanson B, Sakharov BA and Drits VA. *Am Mineral* **90:** 1358-1374 (2005).

[30] Vaia RA and Giannelis EP. *Macromolecules* **30:** 8000-8009 (1997).

[31] Carli LN, Bianchi O, Machado G, Crespo JS and Mauler RS. *Mater Sci Eng C* **33:** 932-937 (2013).

[32] Abe H. *Macromol Biosci* **6:** 469-486 (2006).

[33] Chen DZ, Tang CY, Chan KC, Tsui CP, Yu PHF, Leung MCP and Uskokovic PS. *Compos Sci Technol* **67:** 1617-1626 (2007).

[34] Fukushima K, Tabuani D and Camino G. *Mater Sci Eng C* **29:** 1433-1441 (2009).

[35] Zhang Y-Q, Lee J-H, Rhee JM and Rhee KY. *Compos Sci Technol* **64:** 1383-1389 (2004).

[36] Menard KP. Dynamic mechanical analysis - A practical introduction.CRC Press, Florida, (1999).

[37] Dubnikova IL, Berezina SM, Korolev YM, Kim G-M and Lomakin SM. *J Appl Polym Sci* **105:** 3834-3850 (2007).

[38] Alexandre M, Dubois P, Sun T, Garces JM and Jérôme R. *Polymer* **43:** 2123-2132 (2002).

[39] Hristov VN, Lach R and Grellmann W. *Polym Test* **23:** 581-589 (2004).

[40] Yang J, Wang C-X, Yu Z-S, Li Y, Yang K-K and Wang Y-Z. *J Appl Polym Sci* **121:** 2458-2466 (2011).

[41] Ireland DR. Instrumented impact testing for evaluating end-use performance.American Society for Testing Materials, (1981).

Table 1. Stabilized torque and mechanical energy of PHBV and PHBV nanocomposites.

Sample	Stabilized torque (N m)	Mechanical energy ($kJ\ kg^{-1}$)
PHBV	1.9	384
PHBV/Mt	1.6	375
PHBV/OMt	0.6	270
PHBV/$C_{10}E_3$-Mt	2.0	401

Table 2. DSC and TGA data of PHBV and PHBV nanocomposites.

Sample	DSC data			TGA data		
	T_c (°C)	T_m (°C)	X_c (%)	$T_{5\%}$ (°C)	T_p (°C)	Residue[a] (%)
PHBV	118	165	68	258	283	1.4
PHBV/Mt	119	165	71	261	283	3.6
PHBV/OMt	119	161	69	267	301	3.3
PHBV/$C_{10}E_3$-Mt	119	165	67	259	286	2.8

[a] Determined from TGA curves at 600 °C.